An ensemble method for sensor optimisation applied to falling liquid films

Zhizhao Che[a,*], Fangxin Fang[b], James Percival[b], Christopher Pain[b], Omar Matar[a], Michael Navon[c]

[a]*Department of Chemical Engineering, Imperial College London, UK*
[b]*Department of Earth Science and Engineering, Imperial College London, UK*
[c]*Department of Scientific Computing, Florida State University, US*

Abstract

Multiphase flow problems are often extremely complex due to their strong non-linearity. To study multiphase flow, it is important to simulate or measure key parameters accurately, such as pressure drops and flow rates. Therefore, it is essential to place the sensors at the locations with high impact, and to avoid locations with low impact, where impact is determined by a function such as one of the key variables like pressure drop or flow rate. In this paper, an ensemble method is used to optimise sensor locations for falling film problems based on an importance map. The importance map can identify the important regions according to a target function. The sensor locations are selected based on the importance map, the variation of the variables, and the costs of performing the measurements. We demonstrate the approach by applying data assimilation and show that the optimised sensor locations can significantly improve the data assimilation results. Through sensitivity analysis, sensor optimisation, and data assimilation, this study, for the first time, provides a systematic linkage between the experiments and the models for falling film problems. It also presents a new goal or target based method for sensor placement. This method can be extended to other complex multiphase flow problems.

Keywords: Sensor optimisation, Sensitivity analysis, Falling film, Data

---

*Corresponding author
Email address:* `z.che@imperial.ac.uk` (Zhizhao Che)

assimilation, Adaptive observation

---

1. Introduction

Multiphase flows are characterised by their complexity due to the presence of interfaces and the interaction between different phases. There are many instabilities (Gouesbet and Berlemont, 1993) producing phenomena which have

5 attracted the attention of scientists, engineers, and artists. In numerical simulations and experimental measurements, due to the complexity of the multiphase systems, it is challenging to simulate or measure all the features. With limited resources of simulations and experiments, the problems are often simplified and only the most important features involved in the phenomena are considered.

10 For example, when a liquid slug is moving along a pipe (Hewitt, 1978), many phenomena may occur, such as slug initiation, gas entrainment, and slug propagation. Therefore, researchers often use correlations and closure equations to simplify the problem. Another example is a falling liquid film, which is a common phenomenon not only in industry but also in nature. Researchers have

15 built many low-dimensional models to simplify the falling film problem, e.g., two dimensional models only considering the film evolution along the streamwise direction (Shkadov, 1967), three dimensional models considering the film evolution along the streamwise and the spanwise directions (Scheid et al., 2006). Even after the aforementioned simplification, large volumes of data are often

20 generated in experiments and in simulations. For example, when high speed photography (Thoroddsen et al., 2008) is used to record fast evolving phenomena such as droplet breakup, coalescence, and impact, several gigabytes of data are generated in less than one second. Despite this, researchers are always trying to pursue higher speeds and better resolution of high speed photography in

25 multiphase phenomena.

For complex multiphase problems, it is important that limited resources are used efficiently to capture the most important features. Therefore, it is necessary to define these features, or even better, to develop a method to help

2

researchers determine the most critical features to simulate or to measure. Then
it is possible to use these limited resources to accurately resolve the critical
parts and try to eliminate costs due to unnecessary parts which have negligible
effect. Once the important features are determined, researchers can speed up
simulation by focusing only on the necessary features, and reduce experimental
costs by measuring only the important information.

Whether a feature or a parameter is important depends on the information
we are interested in, or the target. In this paper, we use an ensemble method
to determine the important region for target functions in a falling film problem.
Then the important region is used to optimise the sensor locations in a pseudo
or 'duel-twin' experiment (Bengtsson et al., 1981). Data assimilation (Kalnay,
2003; Evensen, 2003, 2009; Navon, 2009) is then performed to incorporate the
experimental results into the simulation.

The falling film problem is used investigate the use of ensemble methods for
sensitivity analysis, sensor optimisation, and data assimilation. Flow of a falling
liquid film is a phenomenon endowed with rich dynamic features (Chang, 1994;
Chang and Demekhin, 2002; Craster and Matar, 2009; Kalliadasis et al., 2011).
It is characterised by strong nonlinearity, which makes it difficult to simulate
flow qualitatively over long periods. Even though the flow of falling films has
been widely studied in the literature, it still remains a popular research topic and
attracts the attention of mathematicians, physicists, and engineers. Numerical
simulations using the full physics (Gao et al., 2003) or low-dimensional modelling
(Scheid et al., 2006) have been reported. Various aspects of falling films have
been measured experimentally, such as film thickness (Zhou et al., 2009) and
velocity distribution (Adomeit and Renz, 2000). Effects of different influencing
factors in falling films have been studied, such as the effects of thermocapillarity
(Frank and Kabov, 2006), electric fields (Tseluiko and Papageorgiou, 2006),
centrifugal forces (Matar et al., 2005), and surfactants (Strobel and Whitaker,
1969; Ji and Setterwall, 1994). Different processes that may be involved in the
phenomena have been studied, such as heat transfer (Scheid et al., 2008), mass
transfer (Yang and Wood, 1992), chemical reactions (Dabir et al., 1996), and

3

phase change (Palen et al., 1994).

The methods to calculate the sensitivity can be categorised into deterministic methods and statistical methods (Cacuci, 2003; Cacuci et al., 2005). The deterministic methods (Ionescu-Bujor and Cacuci, 2004), such as direct method, FSAP (Forward Sensitivity Analysis Procedure) and ASAP (Adjoint Sensitivity Analysis Procedure), involve differentiation of the system under investigation and exactly computing the sensitivities; while the statistical methods, such as sampling based methods, variance based methods, and FAST (Fourier Amplitude Sensitivity Test), rely on multiple simulations to obtain statistically reliable results (Cacuci and Ionescu-Bujor, 2004). By operating backward in time to describe the propagation of information, adjoint models can be used for sensitivity analysis and adaptive observations (Errico, 1997; Palmer et al., 1998; Baker and Daley, 2000; Daescu and Navon, 2004; Alekseev and Navon, 2010; Godinez and Daescu, 2011). In our previous study, we presented an ensemble method to study the sensitivity (Che et al., 2013), which is simple to implement, and can be used for different target functions for various purposes. In this paper, the method is used to study the sensitivity of a falling liquid film, and then to perform data assimilation based on the optimised sensor locations.

This paper attempts to build a systematic linkage between experimental measurements and numerical simulations through sensitivity analysis, sensor optimisation, and data assimilation. The method presented in this paper can be used not only in falling film problems, but also in a wide range of other applications in multiphase flow. The paper is organised as follows. The methods for the falling film propagation, for sensitivity analysis, and for data assimilation are introduced in Section 2. The dynamic behaviour of falling films, importance maps, optimised sensor locations, as well as comparison among different methods of sensor placement, are discussed in Section 3. In Section 4, conclusions are made and possible extension of this study is discussed.
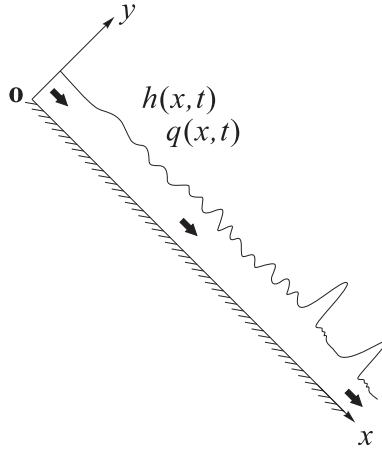
4

Figure 1: Schematic diagram of a falling liquid film flowing down an incline. $h(x,t)$ and $q(x,t)$ are the local transient film thickness and the local transient flow rate, respectively.

2. Method

2.1. Numerical simulation of a falling film

A liquid film flowing down a plane is considered, as shown in Figure 1, the coordinate x is defined along the streamwise direction. The liquid is assumed to be an incompressible Newtonian fluid with constant properties, such as surface tension σ, viscosity μ, and density ρ. A model for the falling film in dimensionless form is (Shkadov, 1967; Chang and Demekhin, 2002; Craster and Matar, 2009)

$$\frac{\partial h}{\partial t} + \frac{\partial q}{\partial x} = 0, \tag{1}$$

$$\frac{\partial q}{\partial t} + \frac{6}{5}\frac{\partial}{\partial x}\left(\frac{q^2}{h}\right) = \frac{1}{5\delta}\left(h\frac{\partial^3 h}{\partial x^3} + h - \frac{q}{h^2}\right), \tag{2}$$

where h and q are, respectively, the dimensionless local film thickness and the dimensionless local flow rate, $\delta = (\rho H_c^{11} g^4/\sigma)^{1/3}/45\nu^2$, and H_c is the film thickness in the absence of waves. It uses a semiparabolic velocity profile and satisfies the no-slip boundary condition at the wall and zero stress boundary condition at the gas-liquid interface. The boundary conditions at the inlet and at the

5

outlet are

$$h = 1, \quad q = 1 \quad \text{at} \quad x = 0, \tag{3}$$

$$\frac{\partial h}{\partial x} = 0, \quad \frac{\partial q}{\partial x} = 0 \quad \text{at} \quad x = L, \tag{4}$$

where $L = 400$ is the length of the domain used for the simulation. L is selected

to be long enough for the development of different types of waves. The initial condition of the falling film is obtained by propagating a uniform liquid film ($h = 1$ and $q = 1$) until the waves in the domain are fully developed.

The falling film equations are discretised using the finite difference method. The transient terms in the falling film equations are integrated using the third order Runge-Kutta method (RK3) (Osher and Fedkiw, 2003). The convective terms are discretised using the total variation diminishing (TVD) scheme (Versteeg and Malalasekera, 2007). The grid size is $\Delta x = 0.5$ and the time step is $\Delta t = 0.005$.

To introduce waves into the problem, noise is added to h at the inlet of the domain to substitute the boundary condition for h in Eq. (3):

$$h(t) = 1 + r(t) \quad \text{at} \quad x = 0, \tag{5}$$

where $r(t)$ is a random number uniformly distributed between -5×10^{-4} and 5×10^{-4}. Tests show that the amplitude of the white noise does not have a significant effect on the overall behaviours of the waves because the noise with resonant wave frequencies will grow exponentially, while other wave frequencies will rapidly be damped.

2.2. Ensemble method for sensitivity analysis

To analyse the sensitivity of the system, a target function F needs to be defined first. The target function can be defined as a scalar considering any variable in the system in the space-time domain, such as the film thickness, the flow rate, the velocity, or the kinetic energy. It should include the information that the researcher is interested in. To quantitatively describe the propagation

6

of information in the system and to identify the important regions in the space-time domain that affect the target function F, here, the sensitivity is defined as the dependence of the variation of the target function F on the variation of the system state Ψ. In a discrete form, the system state Ψ is defined as a column vector containing all the variables for the falling film problem at all nodes, i.e.,

$$\Psi = (h(x_1), h(x_2), h(x_3), ..., h(x_N), q(x_1), q(x_2), q(x_3), ..., h(x_N))^T, \quad (6)$$

where N is the number of nodes used for the simulation, and the superscript T indicates the transpose.

For the dynamic system of a falling film, when the controlling variables deviate from $\mathbf{m}_{\text{exact}}$, the system states deviate from Ψ_{exact}, and correspondingly the target function deviates from F_{exact}. The deviation of the target function F can be approximated using a first order Taylor series expansion:

$$\Delta F \equiv F - F_{\text{exact}} = \frac{\partial F}{\partial \mathbf{m}}(\mathbf{m} - \mathbf{m}_{\text{exact}}) \equiv \frac{\partial F}{\partial \mathbf{m}}\Delta \mathbf{m}. \quad (7)$$

Similarly, the deviation of the system state Ψ can be approximated as:

$$\Delta \Psi \equiv \Psi - \Psi_{\text{exact}} = \frac{\partial \Psi}{\partial \mathbf{m}}(\mathbf{m} - \mathbf{m}_{\text{exact}}) \equiv \frac{\partial \Psi}{\partial \mathbf{m}}\Delta \mathbf{m}. \quad (8)$$

If the system state deviates significantly from the true state Ψ_{exact}, the error introduced by the Taylor series approximation in Eqs. (7–8) might be significant, especially for strongly nonlinear problems.

If we define

$$\mathbf{M} \equiv \frac{\partial \Psi}{\partial \mathbf{m}}, \quad (9)$$

and invert Eq. (8):

$$\Delta \mathbf{m} = \mathbf{M}^{-1}\Delta \Psi \equiv \mathbf{K}\Delta \Psi, \quad (10)$$

with $\mathbf{K} \equiv \mathbf{M}^{-1}$. Substituting Eq. (10) into Eq. (7) yields

$$\Delta F = \frac{\partial F}{\partial \mathbf{m}}\mathbf{K}\Delta \Psi \equiv \mathbf{g}\Delta \Psi, \quad (11)$$

with

$$\mathbf{g} \equiv \frac{\partial F}{\partial \mathbf{m}}\mathbf{K}. \quad (12)$$

Since $\mathbf{g}$ represents the variation of the target function F with the variation of the system state Ψ (as in Eq. (11)), it is referred to as the sensitivity. A large magnitude of sensitivity component $\mathbf{g_i}$ indicates that a small change in Ψ_i will result in a significant variation in F.

Solving Eq. (12) directly is impractical for complex multiphase problems, because the degree of the problem is the number of nodes times the number of variables. The sensitivity, $\mathbf{g}$, can be solved using an ensemble method (Che et al., 2013). An ensemble can be generated by adding perturbations to the system.

The ensemble counterpart of $\mathbf{M}$ is not square and does not possess regular inverse. By introducing the Moore-Penrose pseudoinverse (Moore, 1920) to replace the direct inverse in Eq. (12)

$$\mathbf{K} \equiv (\widehat{\mathbf{M}}^T \widehat{\mathbf{M}})^{-1} \widehat{\mathbf{M}}. \tag{13}$$

Eq. (12) can be rewritten in an ensemble form

$$\hat{\mathbf{g}} \equiv \widehat{\frac{\partial F}{\partial \mathbf{m}_s}} (\widehat{\mathbf{M}_s}^T \widehat{\mathbf{M}_s})^{-1} \widehat{\mathbf{M}_s}^T, \tag{14}$$

where

$$\frac{\partial F}{\partial \mathbf{m}_s} \approx \widehat{\frac{\partial F}{\partial \mathbf{m}_s}} = (F^1 - \overline{F}, F^2 - \overline{F}, F^3 - \overline{F}, ..., F^{\mathcal{E}} - \overline{F}), \tag{15}$$

$$\mathbf{M}_s = \frac{\partial \Psi}{\partial \mathbf{m}_s} \approx \widehat{\mathbf{M}_s} = (\Psi^1 - \overline{\Psi}, \ \Psi^2 - \overline{\Psi}, \ \Psi^3 - \overline{\Psi}, \ ..., \ \Psi^{\mathcal{E}} - \overline{\Psi}), \tag{16}$$

in which $\mathcal{E}$ is the number of ensemble members in the sensitivity analysis. The overbars indicate the ensemble average, and the hats indicate the ensemble counterpart of the matrices.

2.3. EnKF method for data assimilation

Data assimilation was performed using the ensemble Kalman filter (EnKF) method (Evensen, 2003), and its implementation is described briefly here. In the EnKF method, the ensemble is generated by perturbing the inlet boundary condition. The true state of the system is assumed to be known as Ψ_{true}, and it

is used to generate the pseudo experimental data and to validate the assimilation results.

The initial state of the ensemble is stored in matrix $\mathbf{A}$ as

$$\mathbf{A} = (\Psi_1, \Psi_2, \Psi_3, ..., \Psi_N), \tag{17}$$

where N is the number of ensemble members for data assimilation. The ensemble mean $\bar{\mathbf{A}}$ is defined as

$$\bar{\mathbf{A}} = \frac{1}{N} \sum_{i=1}^{N} \Psi_i. \tag{18}$$

Then the ensemble perturbation matrix is

$$\mathbf{A}' = \mathbf{A} - \bar{\mathbf{A}}. \tag{19}$$

The ensemble covariance matrix $\mathbf{P}_e$ is

$$\mathbf{P}_e = \frac{\mathbf{A}'(\mathbf{A}')^T}{N-1}, \tag{20}$$

which indicates the uncertainty of the initial condition.

A vector of measurements $\mathbf{d}$ can be perturbed to generate N vectors of observations as

$$\mathbf{d}_j = \mathbf{d} + \boldsymbol{\epsilon}_j, \tag{21}$$

where $j = 1, ..., N$, and the observation vectors form the observation matrix $\mathbf{D}$

$$\mathbf{D} = (\mathbf{d}_1, \mathbf{d}_2, \mathbf{d}_3, ..., \mathbf{d}_N). \tag{22}$$

The perturbation matrix for observation $\boldsymbol{\gamma}$ is

$$\boldsymbol{\gamma} = (\boldsymbol{\epsilon}_1, \boldsymbol{\epsilon}_2, \boldsymbol{\epsilon}_3, ..., \boldsymbol{\epsilon}_N). \tag{23}$$

Then the measurement error covariance matrix $\mathbf{R}_e$ is

$$\mathbf{R}_e = \frac{\boldsymbol{\gamma}(\boldsymbol{\gamma})^T}{N-1}. \tag{24}$$

The data assimilation procedure minimises the estimated error of the system states based on the initial data $\mathbf{A}$, measurement data $\mathbf{D}$, and their covariances $\mathbf{P}_e$ and $\mathbf{R}_e$, respectively. The analysis equation is

$$\mathbf{A}^a = \mathbf{A} + \mathbf{P}_e \mathbf{H}^T \left(\mathbf{H} \mathbf{P}_e \mathbf{H}^T + \mathbf{R}_e \right)^{-1} \left(\mathbf{D} - \mathbf{H} \mathbf{A} \right), \tag{25}$$

where **H** is the measurement operator, which projects the system state from the model space into the observation space with measurement errors $\boldsymbol{\epsilon}$:

$$\mathbf{d} = \mathbf{H}\Psi + \boldsymbol{\epsilon}. \tag{26}$$

Eq. (25) allows us to update the system state not only at the point of measurement, but also all the variable in the whole domain. It gives a Bayesian estimation of the system state from the experimental data and the numerical data. The details of the EnKF method can be found in Ref. (Evensen, 2003). After the data assimilation step, the analysis results $\mathbf{A^a}$ are optimised by minimising the covariances. Then the ensemble mean of $\mathbf{A^a}$ is used as the updated system state with the uncertainty indicated by the covariance of $\mathbf{A^a}$. The simulation is continued until further experimental data become available for another cycle of data assimilation.

In the data assimilation of falling films, we used a dimensionless interval of data assimilation of $\Delta t = 1$.

3. Results and discussion

3.1. Chaotic behaviour of falling films

The initial profile of the falling film thickness in Figure 2a is used as the true state, and the corresponding profile at $t = 50$ is shown in Figure 2b. The time evolution of h at three typical points, namely $x = 50$, $x = 200$, and $x = 350$, is plotted in Figure 3, which indicates the chaotic feature of the falling film. At $x = 50$, the wave amplitude is so small that it is almost invisible; at $x = 200$, ripples are formed; and at $x = 350$, solitary waves are formed.

3.2. Importance map

An importance map for the falling film problem was generated using the method described in Section 2.2. The importance map is a plot of the sensitivity in the time-space domain. It can provide information about the domain of dependence for the target function and about the propagation of information in
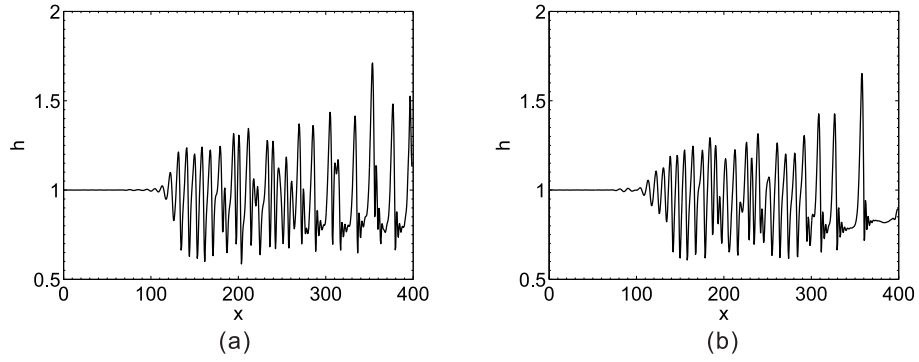
10

Figure 2: The true states of the film thickness h_{true}. (a) Initial true profile of the film thickness at $t = 0$. (b) True profile of the film thickness at $t = 50$.
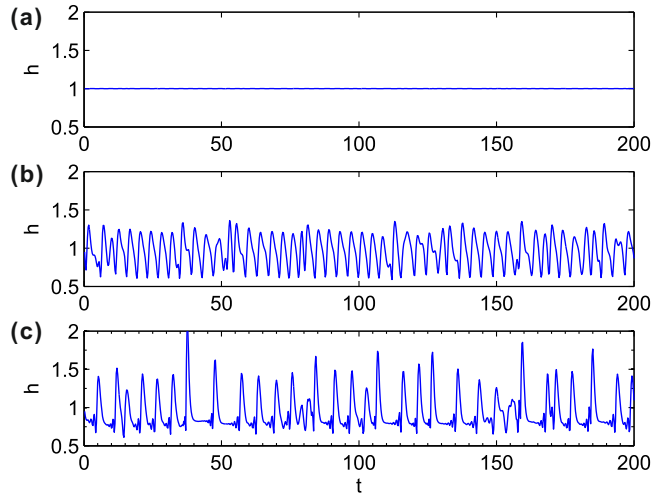

Figure 3: Time evolution of h at three points along the streamwise direction of the falling film: (a) $x = 50$, (b) $x = 200$, (c) $x = 350$.
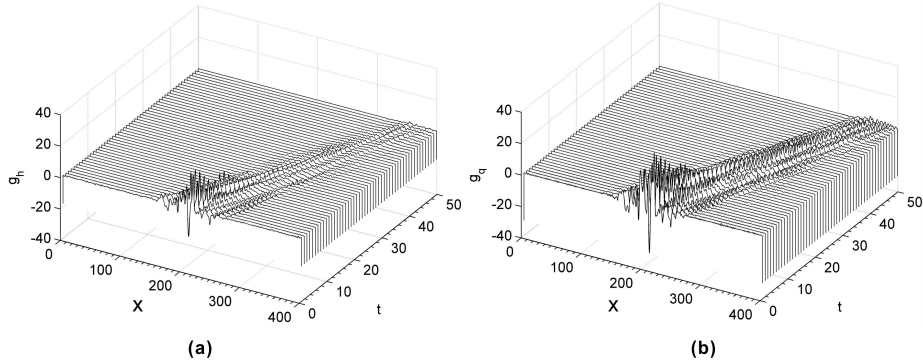
Figure 4: Importance map $g(x,t)$ for the falling film with the definition of the target function for the solitary wave near the outlet of the domain in Figure 2b. (a) Sensitivity of the film thickness h. (b) Sensitivity of the film flow rate q. The target function F is defined in Eqs. (27)–(28) with $\mu = 0.9L$ and $\sigma = 0.05L$.

the time-space domain. The importance map depends on the target function. Here the target function F is defined to capture the solitary wave in the downstream of the domain at $t = 50$, as shown in Figure 2b. A Gaussian function $G(x)$ is used to extract the wave from the whole curve,

$$G(x) = \frac{1}{\sigma\sqrt{2\pi}}e^{-\frac{1}{2}\left(\frac{x-\mu}{\sigma}\right)^2}, \tag{27}$$

$$F = \int_0^L h(x)G(x)dx, \tag{28}$$

where $\mu = 0.9L$ and $\sigma = 0.05L$. From the importance map, it can be seen that information propagates from upstream to downstream with time.

3.3. Variation of variables

A measurement is useful only if the variation of the measured value at that point $\Delta\Psi(x)$ is larger than the sensitivity of the sensors. Even if a small variation at one point may have significant influence on the target, there is no use in allocating a sensor at that point if the sensor could not detect the variation. Here the statistic variation of h and q are plotted in Figure 5 based on the
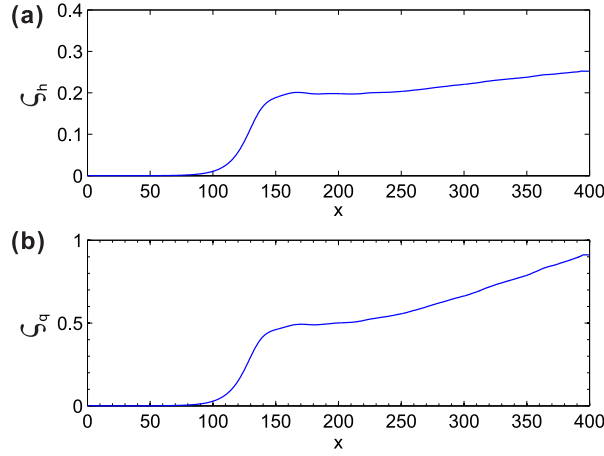
12

Figure 5: Variation of the film thickness and the flow rate along the streamwise direction of the falling film. (a) Variation of the local film thickness ς_h defined in Eq. (29), (b) variation of the local flow rate ς_q defined in Eq. (30).

long-time running of the falling film model,

$$\varsigma_h = \sqrt{\frac{1}{n_t} \sum_{j=1}^{n_t} (h_j - H_c)^2}, \tag{29}$$

$$\varsigma_q = \sqrt{\frac{1}{n_t} \sum_{j=1}^{n_t} (q_j - Q_c)^2}, \tag{30}$$

where h_j and q_j are the transient local film thickness and the transient local flow rate, $H_c = 1$ and $Q_c = 1$ are the film thickness and the flow rate without any wave, j is the index for time step, and n_t is the total number of time steps considered, which should be sufficiently large so that ς_h and ς_q do not significantly change when increasing n_t.

Since there is no variation in the upstream of the falling film, as shown in Figure 5, there is no need to place any sensor in that region. In the downstream, the variation is much larger than that in the upstream, therefore, the probability of observing measurable perturbations to get measurable results is much higher.

13

3.4. Other considerations

In designing experiments, there may be other considerations of sensor placement, e.g., the costs to measure a specific variable at a specific point. The costs can be in terms of money or time. Researchers tend to obtain accurate experimental results while keeping the costs low. A function $c(x, \Psi)$ for the cost of measurement at x for variable Ψ can be defined. Here, for simplicity, it is assumed the cost of measuring the local flow rate of the falling film q is much larger than that of measuring the film thickness h, and the cost of measuring h is the same at different points along the streamwise direction. Other types of costs can be defined and analysed in a similar way.

The sensitivity, $g(x, \Psi)$, as described in Section 3.2, the variation of the variables, $\varsigma(x, \Psi)$, as described in Section 3.3, and the measurement cost, $c(x, \Psi)$, can be considered together by using a combined parameter,

$$\chi(x, \Psi) = \frac{|g(x, \Psi)|\varsigma(x, \Psi)}{c(x, \Psi)}. \tag{31}$$

Then sensor optimisation can be performed simply by finding the area with the largest magnitude of $\chi(x, \Psi)$. Since the sensitivity, g, varies with time, the optimised sensor locations can be adapted correspondingly if sensors are allowed to move. If the strategy of adaptive sensors is challenging to implement in experiments, sensors can be placed considering all time steps, which will result in a strategy with optimised fixed sensors. These strategies are compared in the next section.

3.5. Data assimilation results

Experimental data are necessary to perform data assimilation. The 'dual-twin' experiment is used to generate the synthetic experimental data (Bengtsson et al., 1981): the synthetic experimental data were generated by adding random numbers on the true values [Figure 2], and the random numbers has a Gaussian distribution with a standard deviation depending on the accuracy of sensors.

To form the ensemble for data assimilation using EnKF method, extra noise of smaller covariance than the primary noise was added to the true values. The

number of ensemble members N is 200 for data assimilation. For the ith member of the ensemble,

$$h_i(t) = 1 + r(t) + r_i(t) \quad \text{at} \quad x = 0, \tag{32}$$

where $r_i(t)$ is a random number uniformly distributed $-10^{-4} < r_i < 10^{-4}$. The film thicknesses of the ensemble members have a value close to unity at the inlet, and the noise grows exponentially. As shown in Figure 6a, the ensemble members are completely segregated at the downstream end of the falling film (e.g., $x > 200$) due to the strong nonlinearity of the falling film problem and the exponential growth of perturbations along the streamwise direction. The deviation of the ensemble from the true state can be quantified by

$$\zeta(x) = \sqrt{\frac{1}{N} \sum_{i=1}^{N} (h_i(x) - h_{\text{true}}(x))^2}. \tag{33}$$

The distribution of ζ for the ensemble at the initial state is plotted in Figure 6b.

Three strategies of sensor placement are considered, which are, respectively: (1) uniformly distributed sensors in the whole domain, (2) optimised fixed sensors, and (3) optimised adaptive sensors. Data assimilation is performed using synthetic experimental results based on the three strategies of sensor placement, and the results are compared to those without experimental data for data assimilation, as shown in Figure 7. The comparison shows that the ensemble without data assimilation, due to the strong nonlinearity of the falling film problem, has a very large variance in most of the domain except near the inlet, as shown in Figure 7a. The relatively small variance in the upstream is due to the small perturbation, and the large variation in the downstream is due to the exponential growth of the perturbation. The large variation indicates a large uncertainty of the numerical simulation.

The simulation with uniformly distributed sensors can improve the simulation results in the whole domain [Figure 7b], but the improvement in the region defined for the target function $x = 0.9L = 360$ is less than the one with the optimised fixed sensors, as shown in Figure 7c. In addition, if one were to con-
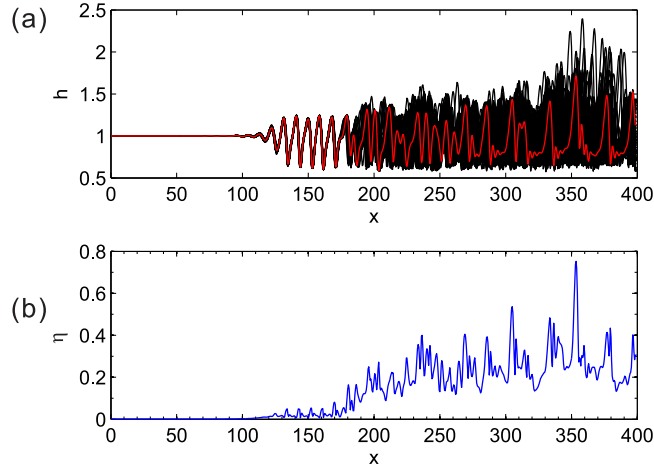
15

Figure 6: (a) Ensemble used for data assimilation (black) and the corresponding true state (red) at $t = 0$. (b) The deviation of the ensemble from the true state defined in Eq. (33).

sider the whole domain, the result with optimised adaptive sensors does not look better than that with optimised fixed sensors. However, if one were to compare the results in the region for the solitary wave $x = 0.9L = 360$, the result with optimised adaptive sensors shows significant improvement in comparison with optimised fixed sensors, as shown in Figure 7d. The ensemble with optimised adaptive sensors can provide the smallest variance in the region defined for the target function, which indicates a small uncertainty of the simulation. The profile of the solitary wave has been well recovered. However, the adaptive sensing strategy requires that the sensors change their locations with time, which might prove to be difficult to achieve for some experiments. The variance in the central region of the domain is larger than that of uniform sensor locations. This is because all the measurements have been allocated to capture the information of the defined target and there is no measurement to capture the overall profile of the falling film. When researchers are interested in the overall profile of the falling film, the target function should be defined across the whole domain.
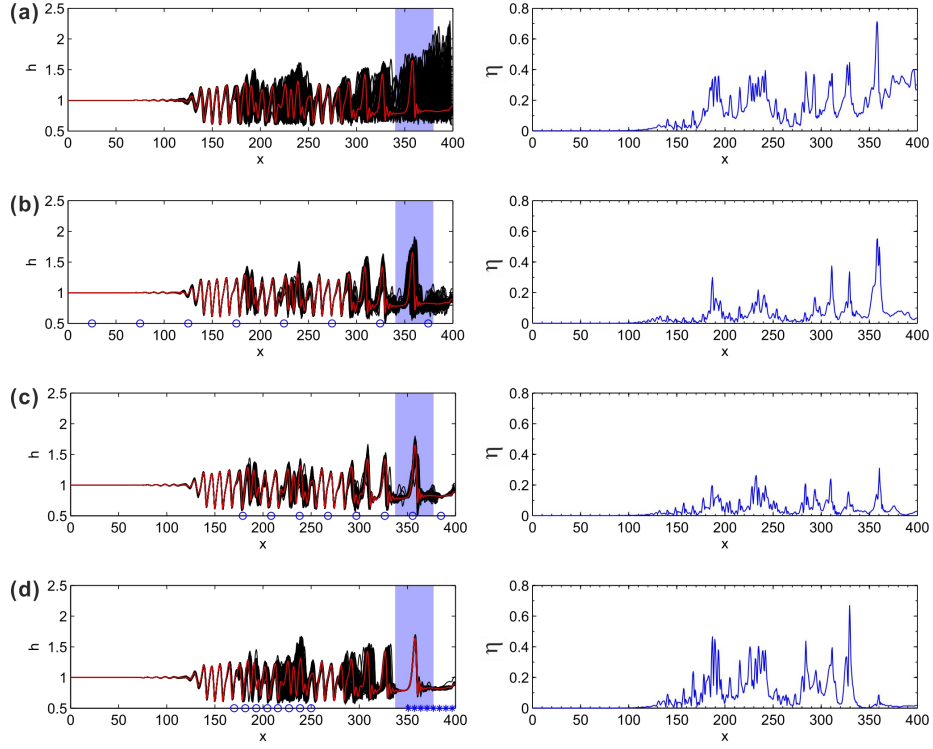
16

Figure 7: Results of data assimilation with different methods of sensor placement. (a) No experimental data for data assimilation, (b) uniformly distributed sensors in the whole domain, (c) optimised fixed sensors, and (d) optimised adaptive sensors. The figures on the left show the profiles of the ensemble (black) and the true state (red), while the figures on the right show the standard deviations from the true states defined in Eq. (33). Eight sensors are used. In (b)-(c), the symbols 'o' along the horizontal axes indicate the location of the sensors. In (d), the symbols 'o' indicate the initial location of the adaptive sensors at $t = 0$, while the symbols '*' indicate the finial location of the adaptive sensors at $t = 50$. $340 < x < 380$ is shaded to highlight the region for the target function defined in Eqs. (27)–(28) with $\mu = 0.9L$ and $\sigma = 0.05L$.

17

3.6. How many sensors are necessary?

In experiments, researchers are not only interested in optimal sensor locations but also in how many sensors are necessary. The number of sensors should be kept low to reduce the costs in installation and maintenance. Here, the effect of number of sensors for the falling film problem is studied by increasing the number of sensors from 1 to 20. The target function is the same as that defined in Section 3.5. Three strategies to place sensors are considered and compared: uniformly distributed sensors in the whole domain, optimised fixed sensors, and optimised adaptive sensors. Data assimilations are performed based on these sensor placement strategies and the results are compared with those obtained without experimental data for assimilation. For a specific application, the required number of sensors depends on the required accuracy. A higher accuracy requires more measurements, and vice versa. For a specific sensor placement strategy, more sensors mean more experimental information can be collected. Therefore, with increasing the number of sensors, the uncertainty of the simulation can be reduced. The improvement becomes insignificant when the number of sensors exceeds a certain value, e.g. 10 optimised adaptive sensors or 15 optimised fixed sensors for the experiments, as shown in Figure 8. Further improvement must be made by other methods, such as using alternative sensors with higher precision.

3.7. A target function for ripples

The optimised sensor locations of measurement are different for different target functions. To capture the ripples in the upstream of the solitary waves, a target function is defined using Eqs. (27)–(28) with $\mu = 0.5L$ and $\sigma = 0.05L$. The corresponding importance map is generated, as shown in Figure 9. The importance map shows that the target function for the ripples is mainly sensitive to the region $0 < x < 200$. However, as shown in Figure 5, the variation of variables near the inlet is too small to be detected. Therefore, the variation must be considered in sensor placement. Even the upstream has a high sensitivity regarding the target function, the inlet region should be avoided because any
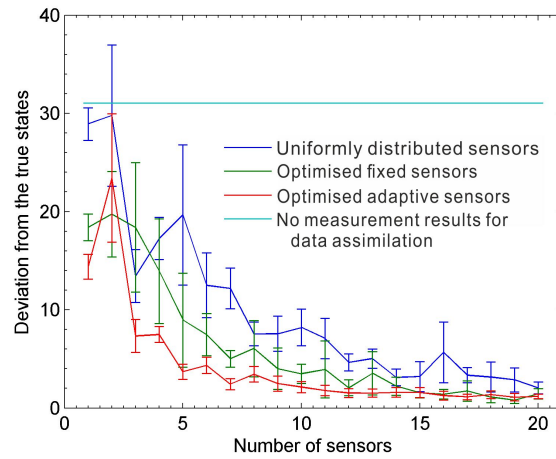
18

Figure 8: Deviation of the target function of the ensemble from the true target function, $\sqrt{\frac{1}{N} \sum_{i=1}^{N} (F_i - F_{\text{true}})^2}$, for data assimilation with different numbers of sensors. Due to the statistical nature of the method, the data assimilation processes were repeated 30 times and the standard deviations are also plotted. The results are improved by increasing the number of sensors. The comparison between the different methods of sensor placement shows the improvement over uniformly distributed sensors. It also shows that the adaptive sensors perform better than the fixed optimised sensors.
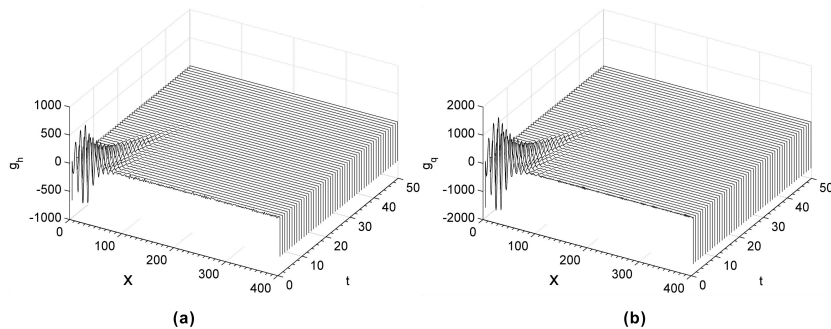
Figure 9: Importance map $g(x,t)$ for the falling film with the definition of the target function for the ripples in Figure 2b. (a) Sensitivity of film thickness h. (b) Sensitivity of film flow rate q. The target function F is defined as Eqs. (27)–(28) with $\mu = 0.5L$ and $\sigma = 0.05L$.

measurement in that region could not detect useful information of the falling film. The results of data assimilation with and without considering the variation are shown in Figure 10. The result without considering the variation is obtained by replacing Eq. (31) with $\chi(x, \Psi) = \frac{|g(x,\Psi)|}{c(x,\Psi)}$. The comparison confirms that the result can be improved when the variation of variables is considered.

4. Conclusions

In this paper, an ensemble method is, for the first time, presented to study the sensitivity of a falling film problem, and the sensitivity is used to optimise the sensor locations. In addition, the new target based sensor placement method is applied with the target of re-producing the film thickness in a region of the domain. The data assimilation study showed that assimilating data from optimised sensor locations can significantly reduce model uncertainty and more accurately reproduce the true system. The data assimilation study also showed that the required number of sensors can be significantly reduced by using optimised sensors.

The sensitivity analysis can identify important parameters and important regions which depend on the target function. The importance map can show the sensitivity of different parameters in the time-space domain. It is not only
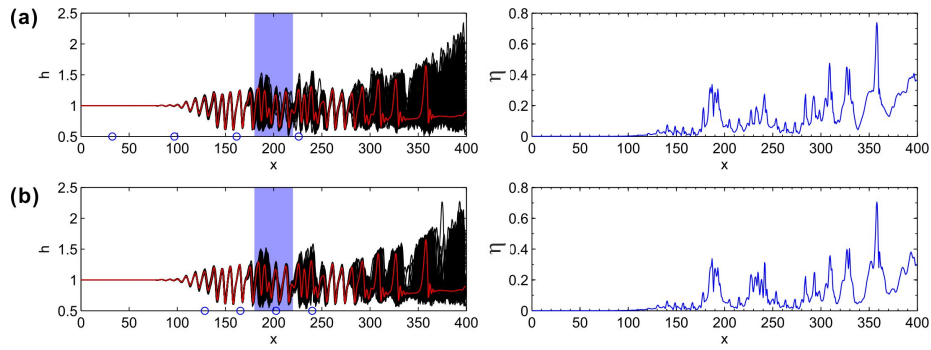
20

Figure 10: Results of data assimilation for a target function of ripples. The target function F is defined as Eqs. (27)–(28) with $\mu = 0.5L$ and $\sigma = 0.05L$. (a) Optimised fixed sensors without considering the variation of variables, i.e., replacing Eq. (31) with $\chi(x, \Psi) = \frac{|g(x,\Psi)|}{c(x,\Psi)}$. The deviation from the true target function is 1.36. (b) Optimised fixed sensors with considering the variation of variables. The deviation from the true target function is 1.16. The figures on the left show the profiles of the ensemble (black) and the true state (red), while the figures on the right show the standard deviation from the true states defined in Eq. (33). Four sensors are used. The symbols 'o' along the horizontal axes indicate the location of the sensors. $180 < x < 220$ is shaded to highlight the region for the target function. The comparison of sensor locations with that in Figure 7 shows the dependency of the sensor location on the target function.

the importance map to be considered to optimised sensor locations, but also the variation of variables and the costs of performing the measurement at d-

³⁵⁵ ifferent locations. Through the sensitivity analysis, sensor optimisation, and data assimilation, this paper provides a systematic linkage between the experiments and the models for falling film problems. This method can be extended to different complex multiphase problems. Through sensitivity studies, the limited resources in experiments and simulations can be focused on regions of high

³⁶⁰ importance to improve the analysis of complex multiphase problems.

References

Adomeit, P., Renz, U., 2000. Hydrodynamics of three-dimensional waves in laminar falling films. International Journal of Multiphase Flow 26, 1183–1208. doi:10.1016/S0301-9322(99)00079-8.

³⁷⁰ Alekseev, A.K., Navon, I.M., 2010. Criteria of optimality for sensors' location based on adjoint transformation of observation data interpolation error. International Journal for Numerical Methods in Fluids 62, 74–89. doi:10.1002/fld.2015.

Baker, N.L., Daley, R., 2000. Observation and background adjoint sensitivity in ³⁷⁵ the adaptive observation-targeting problem. Quarterly Journal of the Royal Meteorological Society 126, 1431–1454. doi:10.1002/qj.49712656511.

Bengtsson, L., Ghil, M., Källén, E., 1981. Dynamic meteorology: Data assimilation methods. Applied mathematical sciences, Springer.

Cacuci, D., 2003. Sensitivity & Uncertainty Analysis: Theory. v. 1, Taylor & Francis.

Cacuci, D., Ionescu-Bujor, M., Navon, I., 2005. Sensitivity and Uncertainty Analysis: Applications to Large-Scale Systems. v. 2, Taylor & Francis.

Cacuci, D.G., Ionescu-Bujor, M., 2004. A comparative review of sensitivity and uncertainty analysis of large-scale systems - ii: Statistical methods. Nuclear Science and Engineering 147, 204–217.

Chang, H., 1994. Wave evolution on a falling film. Annual Review of Fluid Mechanics 26, 103–136. doi:`10.1146/annurev.fl.26.010194.000535`.

Chang, H., Demekhin, E., 2002. Complex Wave Dynamics on Thin Films. Elsevier Science.

Che, Z., Fang, F., Percival, J., Hewitt, G., Pain, C., Matar, O., Navon, M., 2013. An ensemble method for targeted adaptive observations applied to multiphase flows, in: 66th Annual Meeting of the APS Division of Fluid Dynamics, Pittsburgh, Pennsylvania.

Craster, R., Matar, O., 2009. Dynamics and stability of thin liquid films. Reviews of Modern Physics 81, 1131–1198. doi:`10.1103/RevModPhys.81.1131`.

Dabir, B., Riazi, M.R., Davoudirad, H.R., 1996. Modelling of falling film reactors. Chemical Engineering Science 51, 2553–2558. doi:`10.1016/0009-2509(96)00113-3`.

Daescu, D.N., Navon, I.M., 2004. Adaptive observations in the context of 4d-var data assimilation. Meteorology and Atmospheric Physics 85, 205–226. doi:`10.1007/s00703-003-0011-5`.

Errico, R.M., 1997. What is an adjoint model? Bulletin of the American Meteorological Society 78, 2577–2591. doi:`10.1175/1520-0477(1997)078<2577:WIAAM>2.0.CO;2`.

Evensen, G., 2003. The ensemble kalman filter: Theoretical formulation and practical implementation. Ocean Dynamics 53, 343–367. doi:`10.1007/s10236-003-0036-9`.

Evensen, G., 2009. Data Assimilation: The Ensemble Kalman Filter. 2nd ed., Springer.

Frank, A.M., Kabov, O.A., 2006. Thermocapillary structure formation in a falling film: Experiment and calculations. Physics of Fluids 18, 032107. doi:`doi:10.1063/1.2187949`.

Gao, D., Morley, N.B., Dhir, V., 2003. Numerical simulation of wavy falling film flow using vof method. Journal of Computational Physics 192, 624–642. doi:`10.1016/j.jcp.2003.07.013`.

Godinez, H.C., Daescu, D.N., 2011. Observation targeting with a second-order adjoint method for increased predictability. Computational Geosciences 15, 477–488. doi:`10.1007/s10596-010-9217-z`.

Gouesbet, G., Berlemont, A., 1993. Instabilities in multiphase flows. Plenum Press.

Hewitt, G.F., 1978. Measurement of two phase flow parameters. volume 79. Academic Press.

Ionescu-Bujor, M., Cacuci, D.G., 2004. A comparative review of sensitivity and uncertainty analysis of large-scale systems - i: Deterministic methods. Nuclear Science and Engineering 147, 189–203.

Ji, W., Setterwall, F., 1994. On the instabilities of vertical falling liquid films in the presence of surface-active solute. Journal of Fluid Mechanics 278, 297–323. doi:`10.1017/S0022112094003721`.

Kalliadasis, S., Ruyer-Quil, C., Scheid, B., Velarde, M., 2011. Falling Liquid Films. Springer.

Kalnay, E., 2003. Atmospheric Modeling, Data Assimilation and Predictability. Cambridge University Press.

Matar, O.K., Lawrence, C.J., Sisoev, G.M., 2005. The flow of thin liquid films over spinning disks: Hydrodynamics and mass transfer. Physics of Fluids 17, 052102. doi:10.1063/1.1891814.

Moore, E.H., 1920. On the reciprocal of the general algebraic matrix. Bulletin of the American Mathematical Society 26, 394–395. doi:10.1090/S0002-9904-1920-03322-7.

Navon, I., 2009. Data Assimilation for Numerical Weather Prediction: A Review. Springer Berlin Heidelberg. book section 2. pp. 21–65. doi:10.1007/978-3-540-71056-1_2.

Osher, S., Fedkiw, R., 2003. Level Set Methods and Dynamic Implicit Surfaces. Springer.

Palen, J.W., Wang, Q., Chen, J.C., 1994. Falling film evaporation of binary mixtures. AIChE Journal 40, 207–214. doi:10.1002/aic.690400203.

Palmer, T.N., Gelaro, R., Barkmeijer, J., Buizza, R., 1998. Singular vectors, metrics, and adaptive observations. Journal of the Atmospheric Sciences 55, 633–653. doi:10.1175/1520-0469(1998)055<0633:SVMAAO>2.0.CO;2.

Scheid, B., Kalliadasis, S., Ruyer-Quil, C., Colinet, P., 2008. Spontaneous channeling of solitary pulses in heated-film flows. EPL (Europhysics Letters) 84, 64002. doi:10.1209/0295-5075/84/64002.

Scheid, B., Ruyer-Quil, C., Manneville, P., 2006. Wave patterns in film flows: modelling and three-dimensional waves. Journal of Fluid Mechanics 562, 183. doi:10.1017/s0022112006000978.

Shkadov, V.Y., 1967. Wave flow regimes of a thin layer of viscous fluid subject to gravity. Fluid Dynamics 2, 29–34. doi:10.1007/BF01024797.

Strobel, W.J., Whitaker, S., 1969. The effect of surfactants on the flow characteristics of falling liquid films. AIChE Journal 15, 527–532. doi:`10.1002/aic.690150412`.

Thoroddsen, S., Etoh, T., Takehara, K., 2008. High-speed imaging of drops and bubbles. Annual Review of Fluid Mechanics 40, 257–285. doi:`10.1146/annurev.fluid.40.111406.102215`.

Tseluiko, D., Papageorgiou, D.T., 2006. Wave evolution on electrified falling films. Journal of Fluid Mechanics 556, 361–386. doi:`10.1017/S0022112006009712`.

Versteeg, H., Malalasekera, W., 2007. An Introduction to Computational Fluid Dynamics: The Finite Volume Method. Pearson Education Limited.

Yang, R., Wood, B.D., 1992. A numerical modeling of an absorption process on a liquid falling film. Solar Energy 48, 195–198. doi:`10.1016/0038-092X(92)90138-Z`.

Zhou, D.W., Gambaryan-Roisman, T., Stephan, P., 2009. Measurement of water falling film thickness to flat plate using confocal chromatic sensoring technique. Experimental Thermal and Fluid Science 33, 273–283. doi:`10.1016/j.expthermflusci.2008.09.003`.

26